

Flute-Mode Stability of Quadrupole-Anchored Tandem Mirror Plasmas

Hitoshi HOJO

Plasma Research Center, University of Tsukuba, Tsukuba 305-8577, Japan

(Received 10 June 2009 / Accepted 8 January 2010)

We study the flute-mode stability of quadrupole-anchored tandem mirror plasmas. The present analysis is based on Newcomb's Lagrangian density with an assumption of small Larmor radius of ions for paraxial approximation. A radial eigenmode equation for flute perturbations is derived without an eikonal approximation in flux coordinates, where effects of $E \times B$ plasma rotation due to an ambipolar electric field are considered. The obtained eigenmode equation is applicable to a mode with an arbitrary azimuthal mode number and can describe interchange, $E \times B$ rotational, and Kelvin-Helmholtz modes driven by the shear effect of $E \times B$ plasma rotation. A quadratic dispersion equation in perturbation frequency ω is derived based on a simplified cylindrical plasma model and is used to discuss the flute stability of quadrupole-anchored GAMMA 10 tandem mirror plasmas, where the anchor beta required for plasma stability is calculated for the $m = 1$ and 2 modes for different values of central-cell ambipolar potential.

© 2010 The Japan Society of Plasma Science and Nuclear Fusion Research

Keywords: flute-mode stability, tandem mirror plasma, quadrupole-anchor, Newcomb's Lagrangian density, beta value, interchange mode, $E \times B$ rotational mode, Kelvin-Helmholtz mode

DOI: 10.1585/pfr.5.008

1. Introduction

The magnetohydrodynamic (MHD) stability of plasma is very important for achieving a high-beta plasma in tandem mirror fusion research. In a tandem mirror with a minimum- B anchor for MHD stability, such as GAMMA 10, the beta value attainable in a central cell depends strongly on the beta value in an anchor cell and magnitude of an ambipolar electric field [1, 2].

Many studies of MHD stability on a tandem mirror plasma have been reported. However, they have concentrated mainly on studying high- m ballooning modes of a quadrupole-anchored tandem mirror plasma with an eikonal approximation [3–5], and low- m flute and ballooning modes of an axisymmetric tandem mirror plasma [6–8], where m is an azimuthal mode number. Presently in tandem mirror experiments, the MHD stability of a quadrupole-anchored tandem mirror plasma against low- m flute perturbations is the most important concern, because the attained beta values are still low.

In this paper, we study the flute-mode stability of a quadrupole-anchored tandem mirror plasma. The analysis is based on a Lagrangian density developed by Newcomb [9], which assumes the paraxial approximation and small Larmor radius of ions. Starting from Newcomb's Lagrangian density, we derive a radial eigenmode equation for flute-mode perturbations that includes the effects of $E \times B$ plasma rotation due to an ambipolar electric field. The obtained eigenmode equation is applicable to a flute mode with an arbitrary m and can describe interchange, $E \times B$ rotational, and Kelvin-Helmholtz modes driven by

the shear effect of $E \times B$ plasma rotation [10] and ion finite Larmor radius (FLR) stabilizing effect.

In the following section, we derive a radial eigenmode equation for low-frequency flute-mode perturbations in a quadrupole-anchored tandem mirror plasma from Newcomb's Lagrangian density. In Sec. 3, we derive a quadratic dispersion equation in the perturbation frequency ω from the radial eigenmode equation obtained in Sec. 2, assuming a cylindrical plasma model. In Sec. 4, we discuss the flute-mode stability of quadrupole-anchored GAMMA 10 plasmas based on the quadratic dispersion equation in ω , especially the interchange modes, $E \times B$ rotational mode, and ion FLR stabilizing effect.

2. Derivation of Flute Mode Equation

In this section, we study the flute-mode stability of a quadrupole-anchored tandem mirror plasma such as GAMMA 10. The starting point is Newcomb's Lagrangian density [9, 10] in a paraxial approximation, which is given by

$$L = \frac{1}{2} (\rho \mathbf{x}_{,t} \cdot \mathbf{x}_{,t} + S \mathbf{x}_{,t} \cdot \mathbf{x}_{,\theta} - R \mathbf{x}_{,\theta} \cdot \mathbf{x}_{,\theta} - Q \mathbf{x}_{,z} \cdot \mathbf{x}_{,z}), \quad (1)$$

with

$$\begin{aligned} S &= 2\rho\Phi_{,\psi} - (HB^2)_{,\psi}/2B, \\ R &= -\rho\Phi_{,\psi}^2 + (HB^2)_{,\psi}\Phi_{,\psi}/2B - B_{,\psi}K_{,\psi}/B, \\ H &= -8\pi B \sum (M^2/q) \int f\mu d\mu d\varepsilon/|v_{\parallel}|, \end{aligned}$$

$$K = 2\pi B^3 \sum (M^3/q^2) \int f \mu^2 d\mu d\varepsilon / |v_{\parallel}|,$$

$$Q = B^2 + P_{\perp} - P_{\parallel},$$

where $\mathbf{x} = (x, y)$ is the position of a magnetic field line expressed as a function of flux coordinates (ψ, θ, z) , where z is the coordinate along the field line in the paraxial approximation. $\Phi, f, \rho, M, q, P_{\perp}$ (P_{\parallel}), and ε are the ambipolar potential, equilibrium distribution function, equilibrium mass density, mass, charge, perpendicular (parallel) plasma pressure, and particle energy per unit mass, respectively, given by

$$\varepsilon = \mu B + v_{\parallel}^2/2 + q\Phi/M,$$

and μ is the magnetic moment per unit mass, given by

$$\mu = v_{\perp}^2/2B,$$

The subscripts of (ψ, θ, z) and time t accompanied by a comma indicate the partial derivative; that is, $A_{,t} = \partial A/\partial t$ and $A_{,z} = \partial A/\partial z$. In the flux coordinates, the equilibrium magnetic field \mathbf{B} is expressed as

$$\mathbf{B} = B\mathbf{b} = \nabla\psi \times \nabla\theta,$$

where $\mathbf{b} = \mathbf{B}/|B|$.

We now introduce an action integral for the Lagrangian density L under the constraint that perturbations of magnetic field lines are incompressible.

$$I = \int_{t_1}^{t_2} dt \int \frac{d\psi d\theta dz}{B} [L + \lambda(\mathbf{x}_{,\psi} \cdot \mathbf{x}_{,\theta}^* - 1)], \quad (2)$$

where λ is an uncertain coefficient, and $\mathbf{x}^* = \mathbf{x} \times \mathbf{b}$. We now try to find the optimal state of \mathbf{x} in the action integral I . For the deformation of the magnetic field line from \mathbf{x} to $\mathbf{x} + \delta\mathbf{x}$ with $\delta\mathbf{x} = 0$ at t_1 and t_2 , from the stationary condition $\delta I = I(\mathbf{x} + \delta\mathbf{x}) - I(\mathbf{x}) = 0$, we obtain a set of Euler-Lagrange equations,

$$\mathbf{x}_{,\psi} \cdot \mathbf{F} + \lambda_{,\psi} = 0, \quad (3)$$

$$\mathbf{x}_{,\theta} \cdot \mathbf{F} + \lambda_{,\theta} = 0, \quad (4)$$

with

$$\mathbf{F} = \rho\mathbf{x}_{,tt} - B \left[\frac{Q}{B} \mathbf{x}_{,z} \right]_{,z} + S\mathbf{x}_{,t\theta} - R\mathbf{x}_{,\theta\theta}. \quad (5)$$

If we linearize Eqs. (3) and (4) with respect to $\xi = \delta\mathbf{x}$, we obtain

$$\rho\mathbf{x}_{,\psi} \cdot \xi_{,tt} - B\xi_{,\psi} \cdot \left[\frac{Q}{B} \mathbf{x}_{,z} \right]_{,z} - B\mathbf{x}_{,\psi} \cdot \left[\frac{Q}{B} \xi_{,z} \right]_{,z} + S\mathbf{x}_{,\psi} \cdot \xi_{,t\theta} - R\mathbf{x}_{,\psi} \cdot \xi_{,\theta\theta} - R\xi_{,\psi} \cdot \mathbf{x}_{,\theta\theta} + \delta\lambda_{,\psi} = 0, \quad (6)$$

$$\rho\mathbf{x}_{,\theta} \cdot \xi_{,tt} - B\xi_{,\theta} \cdot \left[\frac{Q}{B} \mathbf{x}_{,z} \right]_{,z} - B\mathbf{x}_{,\theta} \cdot \left[\frac{Q}{B} \xi_{,z} \right]_{,z} + S\mathbf{x}_{,\theta} \cdot \xi_{,t\theta} - R\mathbf{x}_{,\theta} \cdot \xi_{,\theta\theta} - R\xi_{,\theta} \cdot \mathbf{x}_{,\theta\theta} + \delta\lambda_{,\theta} = 0. \quad (7)$$

When we introduce ν , defined by

$$\nu = \delta\lambda - B\xi \cdot \left[\frac{Q}{B} \mathbf{x}_{,z} \right]_{,z}, \quad (8)$$

we obtain

$$\nu_{,\psi} = \delta\lambda_{,\psi} - B\xi_{,\psi} \cdot \left[\frac{Q}{B} \mathbf{x}_{,z} \right]_{,z} - \xi \cdot \left[B \left(\frac{Q}{B} \right)_{,z} \mathbf{x}_{,\psi z} + Q_{,\psi} \boldsymbol{\kappa} + Q\boldsymbol{\kappa}_{,\psi} \right], \quad (9)$$

$$\nu_{,\theta} = \delta\lambda_{,\theta} - B\xi_{,\theta} \cdot \left[\frac{Q}{B} \mathbf{x}_{,z} \right]_{,z} - \xi \cdot \left[B \left(\frac{Q}{B} \right)_{,z} \mathbf{x}_{,\theta z} + Q\boldsymbol{\kappa}_{,\theta} \right], \quad (10)$$

where we used $\boldsymbol{\kappa} = \mathbf{x}_{,zz}$, $\boldsymbol{\kappa}$ being the curvature vector, and assumed that $[B(Q/B)_{,z}]_{,\psi} = 0$ and $Q_{,\theta} = 0$. An external magnetic field B_v in vacuum is a function of z only in the paraxial approximation. Thus, in this case, from the axial equilibrium equation in the z direction, we obtain

$$\left[B \left(\frac{Q}{B} \right)_{,z} \right]_{,\psi} = \left(\frac{B^2}{2} + P_{\perp} \right)_{,z\psi} = \left[\frac{B_v^2(z)}{2} \right]_{,z\psi} = 0.$$

Substituting Eqs. (9) and (10) in (7) and (8), we obtain

$$\rho\mathbf{x}_{,\psi} \cdot \xi_{,tt} + Q_{,\psi} \xi \cdot \boldsymbol{\kappa} - B \left[\frac{Q}{B} (\mathbf{x}_{,\psi} \cdot \xi_{,z} - \mathbf{x}_{,\psi z} \cdot \xi) \right]_{,z} + S\mathbf{x}_{,\psi} \cdot \xi_{,t\theta} - R\mathbf{x}_{,\psi} \cdot \xi_{,\theta\theta} + R\xi_{,\psi} \cdot \mathbf{x}_{,\theta\theta} + \nu_{,\psi} = 0, \quad (11)$$

$$\rho\mathbf{x}_{,\theta} \cdot \xi_{,tt} - B \left[\frac{Q}{B} (\mathbf{x}_{,\theta} \cdot \xi_{,z} - \mathbf{x}_{,\theta z} \cdot \xi) \right]_{,z} + S\mathbf{x}_{,\theta} \cdot \xi_{,t\theta} - R\mathbf{x}_{,\theta} \cdot \xi_{,\theta\theta} - R\xi_{,\theta} \cdot \mathbf{x}_{,\theta\theta} + \nu_{,\theta} = 0. \quad (12)$$

If we define $\mathbf{u} = \mathbf{x}_{,\psi}$ and $\mathbf{v} = \mathbf{x}_{,\theta}$, Eqs. (11) and (12) can be rewritten as

$$\rho\mathbf{u} \cdot (\xi_{,tt} + S\xi_{,t\theta} - R\xi_{,\theta\theta}) - R\xi_{,\psi} \cdot \mathbf{v}_{,\theta} + Q_{,\psi} \xi \cdot \boldsymbol{\kappa} - B \left[\frac{Q}{B} (\mathbf{u} \cdot \xi_{,z} - \mathbf{u}_{,z} \cdot \xi) \right]_{,z} + \nu_{,\psi} = 0, \quad (13)$$

$$\rho\mathbf{v} \cdot (\xi_{,tt} + S\xi_{,t\theta} - R\xi_{,\theta\theta}) - R\xi_{,\psi} \cdot \mathbf{v}_{,\theta} - B \left[\frac{Q}{B} (\mathbf{v} \cdot \xi_{,z} - \mathbf{v}_{,z} \cdot \xi) \right]_{,z} + \nu_{,\theta} = 0, \quad (14)$$

If we here express the flute perturbation ξ , as

$$\xi = X\mathbf{u} + Y\mathbf{v} \quad (15)$$

for X and Y we obtain

$$E(\rho X_{,tt} + S X_{,\theta t} - R X_{,\theta\theta}) + F(\rho Y_{,tt} + S Y_{,\theta t} - R Y_{,\theta\theta}) + \frac{F}{2\psi} (S X_{,t} - 2R X_{,\theta}) - 2\psi E (S Y_{,t} - 2R Y_{,\theta}) + 2F R Y + 2\psi E R X_{,\psi} + 2\psi F R Y_{,\psi} - 2\kappa_{\psi} P_{,\psi} X - B \left[\frac{Q}{B} (E X_{,z} + F Y_{,z}) \right]_{,z} + i \frac{Q}{B} Y_{,z} + \nu_{,\psi} = 0, \quad (16)$$

$$F(\rho X_{,tt} + S X_{,\theta t} - R X_{,\theta\theta}) + G(\rho Y_{,tt} + S Y_{,\theta t} - R Y_{,\theta\theta}) + \frac{G}{2\psi} (S X_{,t} - 2R X_{,\theta}) - 2\psi F (S Y_{,t} - 2R Y_{,\theta}) + 2F R Y + 2\psi E R X_{,\theta} + 2\psi F R Y_{,\theta} + (G - 4\psi^2 E) R Y - B \left[\frac{Q}{B} (F X_{,z} + G Y_{,z}) \right]_{,z} - B \left(i \frac{Q}{B^2} X \right)_{,z} + \nu_{,\theta} = 0, \quad (17)$$

where κ_ψ and i are normal components of the curvature and parallel current, respectively, defined by $\kappa_\psi = \mathbf{u} \cdot \boldsymbol{\kappa}$ and

$$i = \mathbf{b} \cdot (\nabla \times \mathbf{b}) = B(\mathbf{u}_{,z} \cdot \mathbf{v} - \mathbf{u} \cdot \mathbf{v}_{,z}). \quad (18)$$

In the derivation of Eq. (16), we used the following relations:

$$\begin{aligned} Q_{,\psi} &= (B^2 + P_\perp - P_\parallel)_{,\psi} = -2P_{\perp,\psi} + (P_\perp - P_\parallel)_{,\psi} \\ &= -2P_{,\psi}, \end{aligned} \quad (19)$$

$$B \left(i \frac{Q}{B^2} \right)_{,z} = 2\kappa_\theta P_{,\psi}, \quad (20)$$

where $\kappa_\theta = \mathbf{v} \cdot \boldsymbol{\kappa}$ is a geodesic component of the curvature. Here, we assume flute-mode perturbations, that is, $X_{,z} = Y_{,z} = 0$. We also assume that physical quantities such as density, pressure, and electrostatic potential are symmetric with respect to the central-cell midplane, so $\rho(-z) = \rho(z)$ and $P(-z) = P(z)$. In this case, if we flute-average Eqs. (16) and (17) and then subtract the ψ -derivative of Eq. (17) from θ -derivative of Eq. (16), we obtain

$$\begin{aligned} &(\langle \rho E \rangle X_{,tt} + \langle S E \rangle X_{,\theta t} - \langle R E \rangle X_{,\theta\theta} - 2\psi \langle S E \rangle Y_{,t} \\ &+ 4\psi \langle R E \rangle Y_{,\theta} + 2\psi \langle R E \rangle X_{,\psi} - 2 \langle \kappa_\psi P_{,\psi} \rangle X)_{,\theta} \\ &- \left(\langle \rho G \rangle Y_{,tt} + \langle S G \rangle Y_{,\theta t} - \langle R G \rangle Y_{,\theta\theta} + \frac{1}{2\psi} \langle S G \rangle X_{,t} \right. \\ &\left. - \frac{1}{\psi} \langle R G \rangle X_{,\theta} + 2\psi \langle R E \rangle X_{,\theta} \right)_{,\psi} = 0, \end{aligned} \quad (21)$$

where flute averaging is defined by

$$\langle A \rangle = \int A \frac{dz}{B},$$

and we used the following relations obtained from the quadrupole symmetry of the magnetic field:

$$\begin{aligned} \langle AE \rangle &= \frac{1}{2\psi} \left\langle A \frac{B_0}{2B^2} \left[\left(\frac{1}{\sigma^2} + \frac{1}{\tau^2} \right) - \left(\frac{1}{\sigma^2} - \frac{1}{\tau^2} \right) \cos 2\theta \right] \right\rangle \\ &= \frac{1}{2\psi} \left\langle A \frac{\sigma^2 + \tau^2}{2B_0} \right\rangle = \frac{1}{2\psi} \langle \langle A \rangle \rangle, \\ \langle AF \rangle &= - \left\langle A \frac{B_0}{2B^2} \left(\frac{1}{\sigma^2} - \frac{1}{\tau^2} \right) \sin 2\theta \right\rangle = 0, \\ \langle AG \rangle &= 2\psi \left\langle A \frac{B_0}{2B^2} \left[\left(\frac{1}{\sigma^2} + \frac{1}{\tau^2} \right) + \left(\frac{1}{\sigma^2} - \frac{1}{\tau^2} \right) \cos 2\theta \right] \right\rangle \\ &= 2\psi \left\langle A \frac{\sigma^2 + \tau^2}{2B_0} \right\rangle = 2\psi \langle \langle A \rangle \rangle. \end{aligned} \quad (22)$$

Using Eq. (22), we can rewrite Eq. (21) as

$$\begin{aligned} &\left[\frac{1}{2\psi} (\langle \langle \rho \rangle \rangle X_{,tt} + \langle \langle S \rangle \rangle X_{,\theta t} - \langle \langle R \rangle \rangle X_{,\theta\theta}) \right. \\ &\left. - \langle \langle S \rangle \rangle Y_{,t} + 2\langle \langle R \rangle \rangle Y_{,\theta} + \langle \langle R \rangle \rangle X_{,\psi} - 2 \langle \kappa_\psi P_{,\psi} \rangle X \right]_{,\theta} \\ &- [2\psi (\langle \langle \rho \rangle \rangle Y_{,tt} + \langle \langle S \rangle \rangle Y_{,\theta t} - \langle \langle R \rangle \rangle Y_{,\theta\theta}) \\ &+ \langle \langle S \rangle \rangle X_{,t} - 2\langle \langle R \rangle \rangle X_{,\theta} + \langle \langle R \rangle \rangle X_{,\theta}]_{,\psi} = 0, \end{aligned} \quad (23)$$

Then, we obtain

$$\begin{aligned} &\frac{1}{2\psi} (\langle \langle \rho \rangle \rangle X_{,tt} + \langle \langle S \rangle \rangle X_{,\theta t} - \langle \langle R \rangle \rangle X_{,\theta\theta})_{,\theta} \\ &- 2 \langle \kappa_\psi P_{,\psi} \rangle X_{,\theta} - [2\psi (\langle \langle \rho \rangle \rangle Y_{,tt} + \langle \langle S \rangle \rangle Y_{,\theta t} \\ &- \langle \langle R \rangle \rangle Y_{,\theta\theta})]_{,\psi} - \langle \langle S \rangle \rangle_{,\psi} X_{,t} + \langle \langle R \rangle \rangle_{,\psi} X_{,\theta} = 0, \end{aligned} \quad (24)$$

where we used the incompressible condition of the flute perturbations, $\nabla \cdot \boldsymbol{\xi} = X_{,\psi} + Y_{,\theta} = 0$. Using the same condition, we have an equation for X as

$$\begin{aligned} &\frac{1}{2\psi} (\langle \langle \rho \rangle \rangle X_{,tt} + \langle \langle S \rangle \rangle X_{,\theta t} - \langle \langle R \rangle \rangle X_{,\theta\theta})_{,\theta\theta} \\ &- 2 \langle \kappa_\psi P_{,\psi} \rangle X_{,\theta\theta} + [2\psi (\langle \langle \rho \rangle \rangle X_{,\psi tt} + \langle \langle S \rangle \rangle X_{,\psi \theta t} \\ &- \langle \langle R \rangle \rangle X_{,\psi \theta\theta})]_{,\psi} - \langle \langle S \rangle \rangle_{,\psi} X_{,t\theta} + \langle \langle R \rangle \rangle_{,\psi} X_{,\theta\theta} = 0. \end{aligned} \quad (25)$$

When we consider flute perturbations as

$$X(\psi, \theta, t) = X(\psi) e^{i(m\theta - \omega t)} + \text{c.c.},$$

we finally obtain a radial eigenmode equation for flute modes,

$$\begin{aligned} &\frac{d}{d\psi} \left[2\psi U \frac{dX}{d\psi} \right] - \frac{m^2}{2\psi} U X + X \frac{d}{d\psi} (m\omega \langle \langle S \rangle \rangle \\ &+ m^2 \langle \langle R \rangle \rangle - 2m^2 \langle P \kappa_\psi \rangle) = 0, \\ &U = \omega^2 \langle \langle \rho \rangle \rangle - m\omega \langle \langle S \rangle \rangle - m^2 \langle \langle R \rangle \rangle, \end{aligned} \quad (26)$$

where S and R for a Maxwellian plasma are given by

$$\begin{aligned} S &= \rho(2\omega_{E \times B} + \omega_{*i}), \\ R &= -\rho\omega_{E \times B}(\omega_{E \times B} + \omega_{*i}), \\ \omega_{E \times B} &= \partial\Phi/\partial\psi, \\ \omega_{*i} &= (M_i/e\rho)\partial P_{\perp i}/\partial\psi, \end{aligned}$$

where $\omega_{E \times B}$ and ω_{*i} are the $E \times B$ drift frequency and ion diamagnetic drift frequency, respectively. Note that the eigenmode in Eq. (26) is derived without an eikonal approximation and thus is applicable to a flute mode with an arbitrary m . It can describe interchange, $E \times B$ rotational, and Kelvin-Helmholtz modes driven by the shear effect of $E \times B$ plasma rotation [10]. Here, we mention that the density and pressure are not symmetric with respect to z , such as $P(-z) \neq P(z)$. In this case, the $\sin 2\theta$ and $\cos 2\theta$ terms arising from the quadrupole magnetic field do not disappear in $\langle AE \rangle$, $\langle AF \rangle$, and $\langle AG \rangle$ in Eq. (22). Also, we obtain coupled mode equations as a radial eigenmode equation, where mode m is coupled with $m \pm 2$ modes.

Finally, we note the relationship between Eq. (26) and familiar Rosenbluth-Simon equation [11], which is derived for a straight magnetic field configuration. If we introduce $\varphi = X/rB$ to replace X , from Eq. (26), we obtain the Rosenbluth-Simon equation as

$$\frac{1}{r} \frac{d}{dr} \left(r^3 U \frac{d\varphi}{dr} \right) + (1 - m^2) U \varphi$$

$$+ \left[\omega^2 r \frac{d\langle \rho \rangle}{dr} - m^2 r \frac{d\langle 2P_{\kappa\psi} \rangle}{dr} \right] \varphi = 0. \quad (27)$$

Multiplying φ^* by Eq. (27) and integrating over r , we obtain a quadratic equation in ω as

$$A_0 \omega^2 - A_1 \omega + A_2 = 0, \quad (28)$$

with

$$\begin{aligned} A_0 &= \int dr \left[r^3 \langle \rho \rangle \left(\left| \frac{d\varphi}{dr} \right|^2 + \frac{m^2 - 1}{r^2} |\varphi|^2 \right) \right. \\ &\quad \left. - r^2 \frac{d\langle \rho \rangle}{dr} |\varphi|^2 \right], \\ A_1 &= \int dr r^3 \langle S \rangle \left(\left| \frac{d\varphi}{dr} \right|^2 + \frac{m^2 - 1}{r^2} |\varphi|^2 \right), \\ A_3 &= \int dr \left[-r^3 \langle R \rangle \left(\left| \frac{d\varphi}{dr} \right|^2 + \frac{m^2 - 1}{r^2} |\varphi|^2 \right) \right. \\ &\quad \left. + r^2 \frac{d\langle 2P_{\kappa\psi} \rangle}{dr} |\varphi|^2 \right]. \quad (29) \end{aligned}$$

Here, if we assume that ρ , S , and R are axially uniform, from $A_2^2 - 4A_1A_3 \geq 0$, which is the stability condition of Eq. (28), we obtain

$$\begin{aligned} \frac{1}{4} \overline{\omega_{*i}^2} &\geq \frac{r}{\rho} \frac{d\langle 2P_{\kappa\psi} \rangle}{dr} \left[1 + \left(-\frac{r}{\rho} \frac{d\rho}{dr} \right) \right] \\ &\quad + \left(-\frac{r}{\rho} \frac{d\rho}{dr} \right) \left(\overline{\omega_{E \times B}^2} + \overline{\omega_{E \times B} \omega_{*i}} \right) \\ &\quad + \overline{(\Delta \omega_{E \times B})^2} + \overline{\Delta \omega_{E \times B} \Delta \omega_{*i}}, \quad (30) \end{aligned}$$

where $\Delta \omega_{E \times B}$, $\Delta \omega_{*i}$ and the average are defined as follows:

$$\begin{aligned} \Delta \omega_{E \times B} &= \omega_{E \times B} - \overline{\omega_{E \times B}}, \quad \Delta \omega_{*i} = \omega_{*i} - \overline{\omega_{*i}}, \\ \bar{A} &= \int dr r^3 \rho \left(\left| \frac{d\varphi}{dr} \right|^2 + \frac{m^2 - 1}{r^2} |\varphi|^2 \right) A \\ &\quad \left/ \int dr r^3 \rho \left(\left| \frac{d\varphi}{dr} \right|^2 + \frac{m^2 - 1}{r^2} |\varphi|^2 \right) \right., \\ \bar{\bar{A}} &= \int dr r \rho |\varphi|^2 A \left/ \int dr r^3 \rho \left(\left| \frac{d\varphi}{dr} \right|^2 + \frac{m^2 - 1}{r^2} |\varphi|^2 \right) \right. \end{aligned} \quad (31)$$

The first, second, and third terms of the right-hand side of Eq. (30) denote the interchange drive, $E \times B$ rotational drive, and Kelvin-Helmholtz drive, respectively. The left-hand side of Eq. (30) expresses the ion FLR stabilization.

3. Stability Analysis for Cylindrical Plasma Model

In this section, we study the stability of a quadrupole-anchored tandem mirror plasma using a cylindrical plasma model for simplicity. Here, we use the long-thin approximation for a mirror plasma. In this approximation, the normal curvature κ_ψ does not depend on ψ . For the density ρ and pressure P , we assume

$$\begin{bmatrix} \rho(z, \psi) \\ P(z, \psi) \end{bmatrix} = \begin{bmatrix} \bar{\rho}(z) \\ \bar{P}(z) \end{bmatrix} \exp\left(-\frac{\psi}{\psi_0}\right), \quad (32)$$

and we also assume that $\omega_{E \times B}$ is a function of z only. If we replace χ with X , defined by

$$\chi = \zeta^{1/2} \exp(-\zeta/2) X, \quad (33)$$

the function χ obeys the following Whittaker equation:

$$\frac{d^2}{d\zeta^2} \chi + \left(-\frac{1}{4} + \frac{\mu}{\zeta} + \frac{1-m^2}{4\zeta^2} \right) \chi = 0, \quad (34)$$

$$\mu = 1 - \frac{\omega^2 \langle \bar{\rho} \rangle - 2m^2 \langle \bar{P}_{\kappa\psi} \rangle}{2[\omega^2 \langle \bar{\rho} \rangle - m\omega \langle \langle \bar{S} \rangle \rangle - m^2 \langle \langle \bar{R} \rangle \rangle]}, \quad (35)$$

where $\langle \langle \bar{S} \rangle \rangle = \langle \langle S(\bar{\rho}, \bar{P}) \rangle \rangle$, $\langle \langle \bar{R} \rangle \rangle = \langle \langle R(\bar{\rho}, \bar{P}) \rangle \rangle$, $\zeta = \psi/\psi_0$ and $\psi_0 = r_p^2 B_0/2$. r_p is the plasma radius of the central-cell plasma, and B_0 is the magnetic field strength of the central cell. If we solve the Whittaker equation under the boundary conditions,

$$\chi(\psi=0) = \text{finite, and } \chi(\psi=\psi_L) = 0, \quad \psi_L = r_L^2 B_0/2 \quad (36)$$

where r_L is the central-cell limiter or wall radius. If we introduce $\eta = 2\mu - 1$ in place of μ , the eigenfunction satisfying the boundary condition is given by

$$\chi(\zeta) = \zeta^{(m+1)/2} \exp(-\zeta/2) M[(m-\eta)/2, 1+m, \zeta], \quad (37)$$

where $M(a, b, z)$ is the Kummer function defined by

$$\begin{aligned} M(a, b, z) &= 1 + \frac{a}{b} z + \frac{a(a+1)}{b(b+1)} \frac{z^2}{2!} \\ &\quad + \frac{a(a+1)(a+2)}{b(b+1)(b+2)} \frac{z^3}{3!} + \dots \end{aligned} \quad (38)$$

The eigenvalue η is determined from $M[(m-\eta)/2, 1+m, \zeta_b] = 0$ with $\zeta_b = (r_L/r_p)^2$ and is expressed as

$$\begin{aligned} \omega^2 - m \left(1 - \frac{1}{\eta} \right) \frac{\langle \bar{\rho} (2\omega_{E \times B} + \omega_{*i}) \rangle}{\langle \langle \bar{\rho} \rangle \rangle} \omega \\ + m^2 \left(1 - \frac{1}{\eta} \right) \frac{\langle \bar{\rho} \omega_{E \times B} (\omega_{E \times B} + \omega_{*i}) \rangle}{\langle \langle \bar{\rho} \rangle \rangle} - \frac{m^2 \langle \bar{P}_{\kappa\psi} \rangle}{\eta \langle \langle \bar{\rho} \rangle \rangle} \\ = 0, \quad (39) \end{aligned}$$

By solving the above quadratic equation in ω , we can discuss the stability of a tandem mirror. When the radius r_L is infinite, the value η is reduced to $\eta = m + 2n$ ($n = 0, 1, 2, \dots$), where n is the radial mode number. When $r_L = \infty$, for the $m = 1$ and $n = 0$ modes, we obtain from Eq. (39)

$$\omega^2 = \langle \bar{P}_{\kappa\psi} \rangle / \langle \langle \bar{\rho} \rangle \rangle. \quad (40)$$

This equation describes the familiar flute interchange stability. The plasma is unstable when $\langle \bar{P}_{\kappa\psi} \rangle$ is negative. Negative κ_ψ corresponds to a so-called bad curvature configuration. On the other hand, when r_L is finite, the second and third terms in Eq. (39) remain and contribute to the stability as the $E \times B$ rotational drive and FLR stabilization, respectively.

4. Stability Analysis of GAMMA 10 Tandem Mirror Plasma

In this section, we discuss the flute-mode stability of GAMMA 10 tandem mirror plasmas based on Eq. (39). Figure 1 shows the right-hand side of the standard magnetic field $B(z)$ in units of tesla and normal curvature $\kappa_\psi(z)$ for the field line of $r = 5$ cm and $\theta = \pi/4$ at the central-cell midplane ($z = 0$), where $B(-z) = B(z)$ and $\kappa_\psi(-z) = \kappa_\psi(z)$. The GAMMA 10 contains five mirror cells: the central cell for ion heating and bulk-plasma production, two anchor cells for MHD stabilization, and two plug/barrier cells for ion-plugging potential formation by strong electron cyclotron resonance heating. The contribution to the plasma stability of the transition-region plasma is considered to be very small, as the flux tube of the transition region is strongly noncircular, and thus the density is low. Here, we assume the following axial profile for pressure $\bar{P}(z) = \bar{P}_\perp + \bar{P}_\parallel$,

$$\bar{P}(z) = \begin{cases} P_0 + P_C \left[1 - \left(\frac{z}{2.8} \right)^2 \right] \exp \left[- \left(\frac{z}{L_C} \right)^2 \right], & 0 \leq |z| \leq 2.8 \\ P_0, & 2.8 \leq |z| \leq 4.4 \\ P_0 + P_A \left[1 - \left(\frac{z-5.2}{0.8} \right)^2 \right] \exp \left[- \left(\frac{z-5.2}{L_A} \right)^2 \right], & 4.4 \leq |z| \leq 6.0 \\ P_0, & 6.0 \leq |z| \leq 7.6 \\ P_0 + P_B \left[1 - \left(\frac{z-8.8}{1.2} \right)^2 \right], & 7.6 \leq |z| \leq 10.0 \end{cases}, \quad (41)$$

where P_0 is a uniform cold-plasma component, and P_C , P_A , and P_B are the peak pressures of mirror-trapped hot components in the central, anchor, and plug/barrier cells,

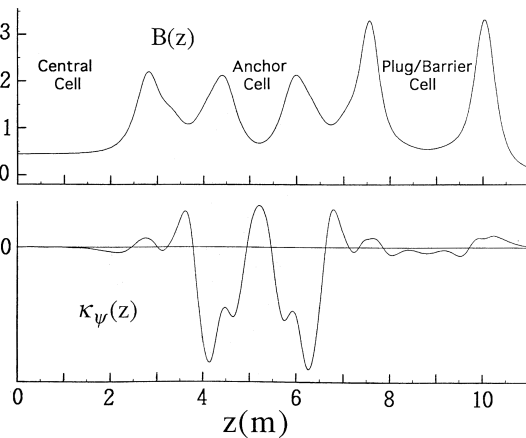


Fig. 1 Standard magnetic field $B(z)$ in units of tesla and normal curvature $\kappa_\psi(z)$ for field line of $r = 5$ cm and $\theta = \pi/4$ at central-cell midplane ($z = 0$), where $B(-z) = B(z)$ and $\kappa_\psi(-z) = \kappa_\psi(z)$.

respectively. L_C and L_A denote the axial extent of the hot components in the central and anchor cells, respectively. If we neglect the contribution from the transition region, $\langle \bar{P}_{\kappa_\psi} \rangle$ is approximately expressed as

$$\langle \bar{P}_{\kappa_\psi} \rangle \approx \langle \bar{P}_{\kappa_\psi} \rangle_A + \langle \bar{P}_{\kappa_\psi} \rangle_C + \langle \bar{P}_{\kappa_\psi} \rangle_B,$$

where $\langle \bar{P}_{\kappa_\psi} \rangle_A$, $\langle \bar{P}_{\kappa_\psi} \rangle_C$, and $\langle \bar{P}_{\kappa_\psi} \rangle_B$ denote integration in the anchor, central, and plug/barrier cells, respectively. The above equation is rewritten as

$$\begin{aligned} \langle \bar{P}_{\kappa_\psi} \rangle &= \frac{B_A^2}{2\mu_0} \left[\beta_A \left\langle \frac{\bar{P}_{\kappa_\psi}}{P_A + P_0} \right\rangle_A - \beta_{CC} \left(\frac{B_C}{B_A} \right)^2 \left| \langle \kappa_\psi \rangle_C \right| \right. \\ &\quad \left. - \beta_{CH} \left(\frac{B_C}{B_A} \right)^2 \left| \left\langle \frac{\bar{P}_{\kappa_\psi}}{P_C} \right\rangle_C \right| - \beta_B \left(\frac{B_B}{B_A} \right)^2 \left| \left\langle \frac{\bar{P}_{\kappa_\psi}}{P_B + P_0} \right\rangle_B \right| \right] \\ &= \frac{B_A^2}{2\mu_0} \left\langle \frac{\bar{P}_{\kappa_\psi}}{P_A + P_0} \right\rangle_A (\beta_A - f_C \beta_{CC} - f_H \beta_{CH} - f_B \beta_B), \end{aligned} \quad (42)$$

where B_A , B_C , and B_B are the midplane magnetic field strengths at the anchor, central, and plug/barrier cells, respectively, and β expresses the peak beta value of each cell (for the central cell, the beta value is divided into the cold-component beta and hot-component beta).

$$\begin{aligned} \beta_A &= \frac{2\mu_0(P_A + P_0)}{B_A^2}, & \beta_{CC} &= \frac{2\mu_0 P_0}{B_C^2}, \\ \beta_{CH} &= \frac{2\mu_0 P_C}{B_C^2}, & \beta_B &= \frac{2\mu_0(P_B + P_0)}{B_B^2}, \\ f_C &= \left(\frac{B_C}{B_A} \right)^2 \left| \langle \kappa_\psi \rangle_C \right| \left| \left\langle \frac{\bar{P}_{\kappa_\psi}}{P_A + P_0} \right\rangle_A \right|, \\ f_H &= \left(\frac{B_C}{B_A} \right)^2 \left| \left\langle \frac{\bar{P}_{\kappa_\psi}}{P_C} \right\rangle_C \right| \left| \left\langle \frac{\bar{P}_{\kappa_\psi}}{P_A + P_0} \right\rangle_A \right|, \\ f_B &= \left(\frac{B_B}{B_A} \right)^2 \left| \left\langle \frac{\bar{P}_{\kappa_\psi}}{P_B + P_0} \right\rangle_B \right| \left| \left\langle \frac{\bar{P}_{\kappa_\psi}}{P_A + P_0} \right\rangle_A \right|. \end{aligned} \quad (43)$$

Figures 2 (a), (b), and (c) show the values of f_C , f_B , and f_H in Eq. (42): f_C as a function of L_A in Fig. 2 (a), f_B as a function of L_A in Fig. 2 (b), and f_H as a function of L_C for two different values of L_A in Fig. 2 (c). These figures show that f_H is much smaller than f_C . This is because the bad-curvature region of the central cell is localized near the mirror throat region, whereas the mirror-trapped hot-component is under low pressure near the mirror throat region. As the central-cell peak beta is given by $\beta_C = 2\mu_0(P_C + P_0)/B_C^2$, when we use β_C , $f_C \beta_{CC} + f_H \beta_{CH}$ is expressed as

$$\begin{aligned} f_C \beta_{CC} + f_H \beta_{CH} &= f_C^* \beta_C, \\ f_C^* &= f_C \frac{P_0}{P_C + P_0} + f_H \frac{P_C}{P_C + P_0}. \end{aligned} \quad (44)$$

Next, we estimate $\langle \langle \bar{\rho} \rangle \rangle$ in Eq. (39).

$$\langle \langle \bar{\rho} \rangle \rangle \approx \left\langle \frac{\bar{\rho}}{B} \right\rangle = \int dz \frac{M_i n}{B^2}$$

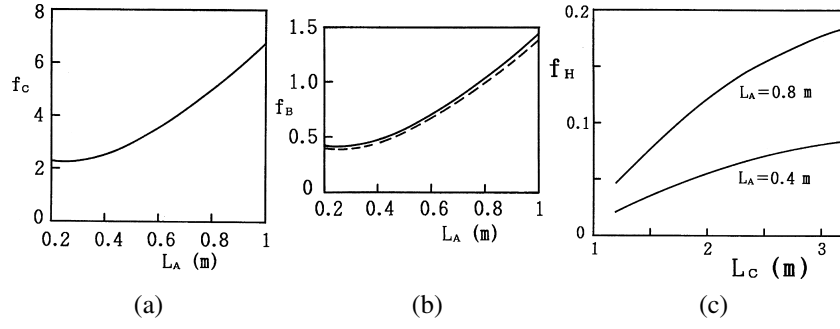


Fig. 2 f_C , f_B , and f_H in Eq. (42). (a): f_C as a function of L_A , (b): f_B as a function of L_A , (c): f_H as a function of L_C for two different values of L_A . It is shown that $f_H \ll f_C$.

$$\begin{aligned}
 &\approx M_i n_C \frac{L_C}{B_C^2} \left[1 + \left(\frac{B_C}{B_A} \right)^2 \frac{2L_A n_A}{L_C n_C} \right. \\
 &\quad \left. + \left(\frac{B_C}{B_B} \right)^2 \frac{2L_B n_B}{L_C n_C} + \left(\frac{B_C}{B_{TR}} \right)^2 \frac{2L_{TR} n_{TR}}{L_C n_C} \right] \\
 &\approx M_i n_C \frac{L_C}{B_C^2} \left[1 + \left(\frac{B_C}{B_A} \right)^2 \frac{2L_A n_A}{L_C n_C} \right. \\
 &\quad \left. + \left(\frac{B_C}{B_B} \right)^2 \frac{2L_B n_B}{L_C n_C} \right], \quad (45)
 \end{aligned}$$

where the contribution from the transition cell is neglected because $(B_{TR}/B_C)^2 > 5$ and $n_{TR} \ll n_C$. If we use the parameters $(B_A/B_C)^2 = 2.28$, $(B_B/B_C)^2 = 1.50$, $L_C = 5.6$ m, $L_A = 1.6$ m, and $L_B = 2.4$ m, we obtain

$$\begin{aligned}
 \langle\langle \bar{\rho} \rangle\rangle &\approx M_i n_C \frac{L_C}{B_C^2} \left[1 + 0.25 \frac{n_A}{n_C} + 0.57 \frac{n_B}{n_C} \right] \\
 &= \delta M_i n_C \frac{L_C}{B_C^2}, \quad (46)
 \end{aligned}$$

where $\delta \approx 1.3$, as $n_B \ll n_C \approx n_A$ is usually obtained experimentally. Then, the interchange drive is expressed as

$$\begin{aligned}
 \Gamma_{\text{MHD}}^2 &= \frac{\langle \bar{P} \kappa_\psi \rangle}{\langle\langle \bar{\rho} \rangle\rangle} \\
 &= \frac{B_A^2 / 2\mu_0}{\delta M_i n_C L_C / B_C^2} \left\langle \frac{\bar{P} \kappa_\psi}{P_A + P_0} \right\rangle_A \\
 &\quad \times (\beta_A - f_C^* \beta_C - f_B \beta_B), \quad (47)
 \end{aligned}$$

where the parameters $B_C = 4.45$ kG, $B_A = 6.73$ kG, and $M_i = 1.67 \times 10^{-27}$ kg are used. We also use the following approximation in the second and third terms of Eq. (39):

$$\begin{aligned}
 \frac{\langle\langle \bar{\rho} (2\omega_{E \times B} + \omega_{*i}) \rangle\rangle}{\langle\langle \bar{\rho} \rangle\rangle} &\approx \frac{\int \frac{dz}{B} \frac{\bar{\rho}}{B} (2\omega_{E \times B} + \omega_{*i})}{\frac{\delta M_i n_C L_C}{B_C^2}} \\
 &= \frac{M_i n_C L_C}{B_C^2} \frac{(2\omega_{E \times B} + \omega_{*i})}{\frac{\delta M_i n_C L_C}{B_C^2}}
 \end{aligned}$$

$$\begin{aligned}
 &= \frac{1}{\delta} (2\omega_{E \times B} + \omega_{*i}), \\
 \frac{\langle\langle \bar{\rho} \omega_{E \times B} (\omega_{E \times B} + \omega_{*i}) \rangle\rangle}{\langle\langle \bar{\rho} \rangle\rangle} &\approx \frac{\int \frac{dz}{B} \frac{\bar{\rho}}{B} \omega_{E \times B} (\omega_{E \times B} + \omega_{*i})}{\frac{\delta M_i n_C L_C}{B_C^2}} \\
 &\approx \frac{1}{\delta} \omega_{E \times B} (\omega_{E \times B} + \omega_{*i}),
 \end{aligned}$$

which is reasonable because the $E \times B$ drift and ion diamagnetic drift frequencies in the central cell are more dominant as compared to those in the other cells in experiments. In this case, Eq. (39) is approximated as

$$\begin{aligned}
 \omega^2 - m \left(1 - \frac{1}{\eta} \right) \frac{1}{\delta} (2\omega_{E \times B} + \omega_{*i}) \omega \\
 + m^2 \left(1 - \frac{1}{\eta} \right) \frac{1}{\delta} \omega_{E \times B} (\omega_{E \times B} + \omega_{*i}) - \frac{m^2}{\eta} \Gamma_{\text{MHD}}^2 = 0, \quad (48)
 \end{aligned}$$

From the stability condition, we obtain

$$\begin{aligned}
 \frac{1}{4} \omega_{*i}^2 \geq \frac{\eta(\delta - 1) + 1}{\eta - 1} \omega_{E \times B} (\omega_{E \times B} + \omega_{*i}) \\
 - \frac{\eta \delta^2}{(\eta - 1)^2} \Gamma_{\text{MHD}}^2. \quad (49)
 \end{aligned}$$

Here, we discuss the ion FLR stabilization of the $E \times B$ rotational mode, which is observed in GAMMA 10 experiments [2, 12]. We then assume that the interchange mode is marginally stable; that is, $\Gamma_{\text{MHD}}^2 = 0$. In this case, from Eq. (49), the ion FLR stabilization condition for the $E \times B$ rotational mode is given by

$$\frac{\omega_{*i}}{\omega_{E \times B}} \geq 2 \frac{\eta(\delta - 1) + 1}{\eta - 1} \left[1 + \sqrt{1 + \frac{\eta - 1}{\eta(\delta - 1) + 1}} \right]. \quad (50)$$

When $(r_L/r_p)^2 = 6.0$, we have $\eta = 1.125$ for the $m = 1$ mode from Eq. (34) with the boundary condition in Eq. (36). If we assume $\delta = 1.3$, we obtain $\omega_{*i}/\omega_{E \times B} > 43.8$ as the FLR stabilization condition of the $E \times B$ rotational

mode. We now discuss the total stability condition of the plasma. With the use of Eq. (47), Eq. (49) is rewritten as

$$\begin{aligned} \beta_A \geq & f_C^* \beta_C + f_B \beta_B \\ & + \frac{(\eta - 1)[\eta(\delta - 1) + 1]}{A\eta\delta^2} \omega_{E \times B} (\omega_{E \times B} + \omega_{*i}) \\ & - \frac{(\eta - 1)^2}{4A\eta\delta^2} \omega_{*i}^2, \end{aligned} \quad (51)$$

where A is given by

$$A = \frac{B_A^2/2\mu_0}{\delta M_i n_C L_C / B_C^2} \chi_A, \quad \chi_A = \left\langle \frac{\bar{P}_{\kappa\psi}}{P_A + P_0} \right\rangle_A. \quad (52)$$

In the stability condition of Eq. (51), the first and second terms of the right-hand side are due to the interchange modes, the third term expresses the $E \times B$ rotational-mode drive, and final term denotes the ion FLR stabilization. We first estimate the value of f_C^* related to the flute interchange modes. The experimental value $f_C^* = 0.25$ reported in Ref. [2] can be explained theoretically. From Fig. 2, we obtain $f_C = 2.5$ for $L_A = 0.4$ and $f_H = 0.054$ for $L_A = 0.4$ and $L_C = 2.0$. Then, using these parameters and Eq. (44), we obtain $f_C^* = 0.24 \sim 0.26$ if we assume $P_C/P_0 = 11 \sim 12$. This pressure ratio P_C/P_0 has been realized in the ion cyclotron range of frequency (ICRF) start-up operation mode of GAMMA 10 experiments [13], and the theoretical value of f_C^* is comparable to the experimental value $f_C^* = 0.25$. For numerical calculations, we estimate the $E \times B$ drift and ion diamagnetic drift frequencies as

$$\omega_{E \times B} = -\frac{\Phi_0}{\psi_L} = -\frac{2\Phi_0 [\text{V}]}{r_L^2 [\text{m}] B_C [\text{T}]}, \quad (53)$$

$$\omega_{*i} = -\frac{M_i P_{\perp i}}{e\rho\psi_0} = -\frac{2T_{\perp i} [\text{eV}]}{r_p^2 [\text{m}] B_C [\text{T}]}. \quad (54)$$

In this case, with the use of Eqs. (52), (53), and (54), Eq. (51) is rewritten as

$$\begin{aligned} \beta_A \geq & f_C^* \beta_C + f_B \beta_B + \frac{(n - 1)[\eta(\delta - 1) + 1]}{\eta\delta \frac{B_A^2}{2\mu_0} \chi_A} \\ & \times \frac{M_i n_C L_C}{B_C^2} \left(\frac{2\Phi_0}{r_p^2 B_C} \right)^2 \left(\frac{r_p}{r_L} \right)^2 \left[\left(\frac{r_p}{r_L} \right)^2 + \frac{T_{\perp i}}{\Phi_0} \right] \\ & - \frac{(\eta - 1)^2}{4\eta\delta \frac{B_A^2}{2\mu_0} \chi_A} \frac{M_i n_C L_C}{B_C^2} \left(\frac{2T_{\perp i}}{r_p^2 B_C} \right)^2, \end{aligned} \quad (55)$$

If we again use the parameters $B_C = 4.45$ kG, $B_A = 6.73$ kG, $M_i = 1.67 \times 10^{-27}$ kg, $L_C = 5.6$ m, and $r_p = 0.1$ m, Eq. (55) is reduced to

$$\begin{aligned} \beta_A \geq & f_C^* \beta_C + f_B \beta_B \\ & + 0.53 \times 10^{-29} \frac{(\eta - 1)[\eta(\delta - 1) + 1]}{\eta\delta \chi_A} \\ & \times \left[1 + \left(\frac{r_L}{r_p} \right)^2 \frac{T_{\perp i} [\text{eV}]}{\Phi_0 [\text{V}]} \right] \frac{n [\text{m}^{-3}]}{r_p^4 [\text{m}]} \Phi_0^2 [\text{V}] \end{aligned}$$

$$- 0.13 \times 10^{-29} \frac{(\eta - 1)^2 n [\text{m}^{-3}]}{\eta\delta \chi_A} \frac{n [\text{m}^{-3}]}{r_p^4 [\text{m}]} T_{\perp i}^2 [\text{eV}]. \quad (56)$$

Here, we consider the case in which the plug/barrier plasma is negligible, and assume $\beta_B = 0$. In this case, as the central-cell beta is approximated by $\beta_C \approx 2\mu_0 n_C T_{\perp i} / B_C^2$, Eq. (56) is rewritten as

$$\begin{aligned} \frac{\beta_A}{n_C} \geq & 2.0 \times 10^{-24} f_C^* T_{\perp i} \\ & + 0.53 \times 10^{-29} C_1 \left[1 + \left(\frac{r_L}{r_p} \right)^2 \frac{T_{\perp i}}{\Phi_0} \right] \frac{1}{r_L^4} \Phi_0^2 \\ & - 0.13 \times 10^{-29} C_2 \frac{1}{r_p^4} T_{\perp i}^2, \end{aligned} \quad (57)$$

with $C_1 = \frac{(\eta - 1)[\eta(\delta - 1) + 1]}{\eta\delta \chi_A}$, $C_2 = \frac{(\eta - 1)^2}{\eta\delta \chi_A}$ and n_C is measured by m^{-3} , $T_{\perp i}$ by eV, and Φ_0 by V, respectively. Calculating Eq. (57), we estimate the anchor-cell beta β_A required for MHD stability of the plasma. In estimating Eq. (56), we assume $\delta = 1.3$ and $f_C^* = 0.25$. The typical value of the central-cell potential Φ_0 in the ICRF start-up operation is $\Phi_0 = 0.5 \sim 1.0$ kV. From the numerical calculation in Ref. [1], we see that χ_A is typically estimated to be $3 < \chi_A < 11$, which depends on the axial pressure profile of the anchor cell. The central-cell limiter radius is $r_L = 18$ cm. When the plasma radius (in pressure) is $r_p = 6.0$ cm, $(r_L/r_p)^2 = 9.0$, and as the eigenvalue of the radial flute-mode equation (Eq. (34)), we have $\eta = 1.015$ and 2.058 for the $m = 1$ and 2 modes, respectively. For $r_p = 7.35$ cm, $(r_L/r_p)^2 = 6.0$, and we have $\eta = 1.125$ for the $m = 1$ and $\eta = 2.350$ for the $m = 2$ mode.

We first discuss the case of $r_p = 6.0$ cm. Figure 3 shows the stability boundary on β_A/n_C of the $m = 1$ mode as a function of $T_{\perp i}$ in keV for $\Phi_0 = 1.0$ kV and $\chi_A = 5.0$ (blue line) and 10.0 (red line), where the dashed line indicates the interchange-mode stability boundary $\beta_A = f_C^* \beta_C$. We see that the anchor beta for stability increases due to the $E \times B$ rotational-mode drive as compared with the

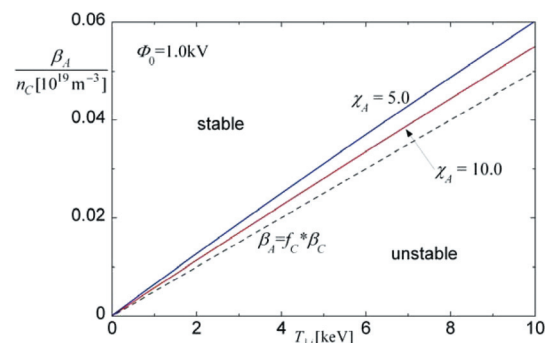


Fig. 3 Stability boundary on β_A of $m = 1$ mode as a function of $T_{\perp i}$ for $\Phi_0 = 1.0$ kV and $\chi_A = 5.0$ (blue) and 10.0 (red), where $r_p = 6$ cm, $r_L = 18$ cm, $\delta = 1.3$, and $f_C^* = 0.25$ are assumed.

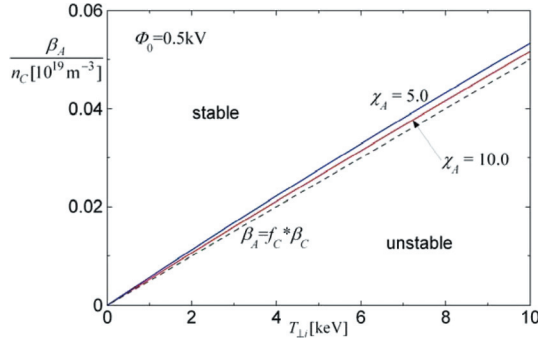


Fig. 4 Stability boundary on β_A of $m = 1$ mode as a function of $T_{\perp i}$ for $\Phi_0 = 0.5$ kV and $\chi_A = 5.0$ (blue) and 10.0 (red), where other parameters are same as those in Fig. 3.

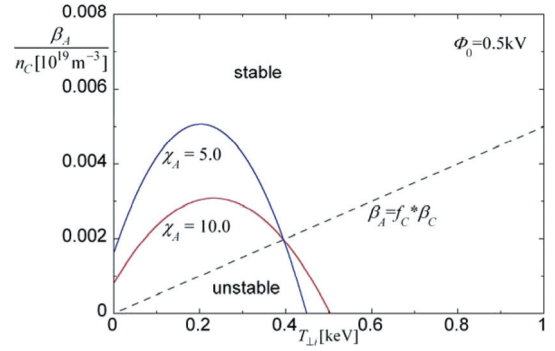


Fig. 6 Stability boundary on β_A of $m = 2$ mode as a function of $T_{\perp i}$ for $\Phi_0 = 0.5$ kV and $\chi_A = 5.0$ (blue) and 10.0 (red), where other parameters are the same as those in Fig. 3.

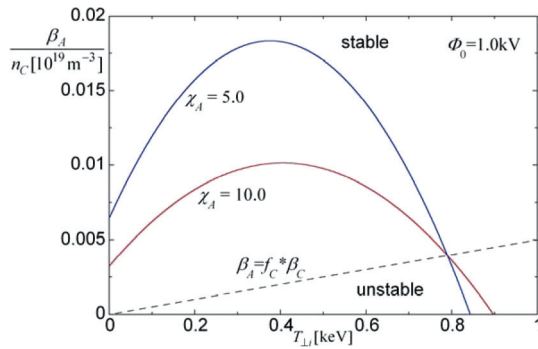


Fig. 5 Stability boundary on β_A of $m = 2$ mode as a function of $T_{\perp i}$ for $\Phi_0 = 1.0$ kV and $\chi_A = 5.0$ (blue) and 10.0 (red), where other parameters are the same as those in Fig. 3.

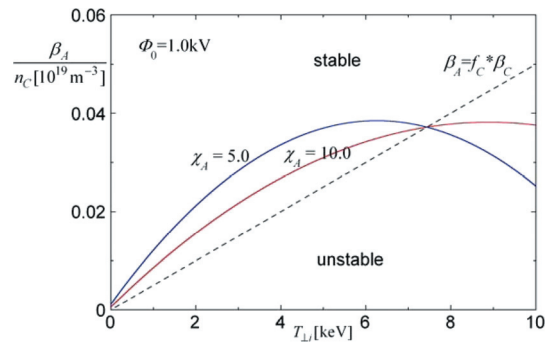


Fig. 7 Stability boundary on β_A of $m = 1$ mode as a function of $T_{\perp i}$ for $\Phi_0 = 1.0$ kV and $\chi_A = 5.0$ (blue) and 10.0 (red), where $r_p = 7.35$ cm, $r_L = 18$ cm, $\delta = 1.3$, and $f_C = 0.25$ are assumed.

interchange-mode stability boundary. This anchor-beta increase for stability is consistent with GAMMA 10 experiments [2, 14]. We also see that in this case, the ion FLR stabilizing effect is negligibly small ($T_{\perp i} = 10$ keV, as the term is proportional to $T_{\perp i}^2$). Figure 4 shows the stability boundary on β_A/n_C of the $m = 1$ mode as a function of $T_{\perp i}$ in keV for $\Phi_0 = 0.5$ kV, where the other parameters are the same as those in Fig. 3. The anchor-beta increase for stability due to the $E \times B$ rotational-mode drive is smaller than that in Fig. 3. Figure 5 shows the stability boundary on β_A/n_C of the $m = 2$ mode as a function of $T_{\perp i}$ for $\Phi_0 = 1.0$ kV, and Fig. 6 shows the stability boundary on β_A/n_C of the $m = 2$ mode as a function of $T_{\perp i}$ for $\Phi_0 = 0.5$ kV, where the other parameters are the same as those in Fig. 3. For both cases, though the anchor-beta increase for stability due to the $E \times B$ rotational-mode drive is larger than that in Figs. 3 and 4, the plasma can be completely stabilized by the ion FLR effect when the ion temperature $T_{\perp i}$ increases. Ion FLR stabilization is more effective for smaller Φ_0 . Therefore, we see that when the plasma radius is small, the $m = 1$ is less stable than $m = 2$ mode.

We next discuss the case of $r_p = 7.35$ cm. Figure 7 shows the stability boundary on β_A/n_C of the $m = 1$ mode

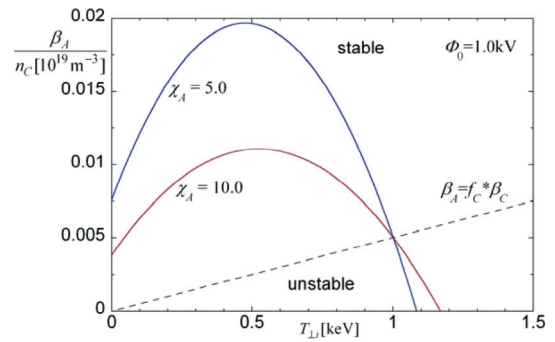


Fig. 8 Stability boundary on β_A of $m = 2$ mode as a function of $T_{\perp i}$ for $\Phi_0 = 1.0$ kV and $\chi_A = 5.0$ (blue) and 10.0 (red), where other parameters are same as those in Fig. 7.

as a function of $T_{\perp i}$ in keV for $\Phi_0 = 1.0$ kV and $\chi_A = 5.0$ (blue line) and 10.0 (red line), where the dashed line indicates the interchange-mode stability boundary $\beta_A = f_C^* \beta_C$. In this case, we find that the ion FLR stabilizing term becomes effective when the ion temperature $T_{\perp i}$ increases compared with Fig. 3. Figure 8 shows the stability boundary on β_A/n_C of the $m = 2$ mode as a function of $T_{\perp i}$ for

$\Phi_0 = 1.0$ kV, where the other parameters are the same as those in Fig. 7. Figure 8 is similar to Fig. 5 for $m = 2$ at $r_p = 6.0$ cm. This is because $\eta = 2.350$ for the $m = 2$ mode at $r_p = 7.35$ cm is relatively close to $\eta = 2.058$ for the $m = 2$ mode at $r_p = 6.0$ cm. Nonetheless, we see from these figures that the $m = 2$ modes are more strongly stabilized by the ion FLR effect than the $m = 1$ modes.

Acknowledgement

This work was partly supported by a Grant-in-Aid for Scientific Research from the Ministry of Education, Culture, Sports, Science and Technology of Japan. The author thanks the members of the Plasma Research Center, University of Tsukuba for useful discussion.

Appendix.

In this Appendix, we derive the relations for a vacuum quadrupole magnetic field. The vacuum quadrupole magnetic field in the paraxial approximation is expressed by

$$\mathbf{x} = \begin{pmatrix} x \\ y \end{pmatrix} = \begin{pmatrix} x_0 \sigma(z) \\ y_0 \tau(z) \end{pmatrix},$$

$$x_0 = \sqrt{\frac{2\psi}{\beta_0}} \cos(\theta), \quad y_0 = \sqrt{\frac{2\psi}{\beta_0}} \sin(\theta), \quad (\text{A.1})$$

with $\sigma(-z) = -\tau(z)$ for quadrupole symmetry. For the above magnetic field line, we obtain the following relations:

$$\mathbf{u} = \mathbf{x}_{,\psi} = \frac{\mathbf{x}}{2\psi}, \quad \mathbf{v} = \mathbf{x}_{,\theta} = \begin{pmatrix} -y_0 \sigma \\ x_0 \tau \end{pmatrix},$$

$$\mathbf{u}_{,\psi} = \mathbf{x}_{,\psi\psi} = -\frac{\mathbf{u}}{2\psi}, \quad \mathbf{v}_{,\psi} = \mathbf{x}_{,\theta\psi} = \frac{\mathbf{v}}{2\psi},$$

$$\mathbf{u}_{,\theta} = \mathbf{x}_{,\psi\theta} = \frac{\mathbf{v}}{2\psi}, \quad \mathbf{v}_{,\theta} = \mathbf{x}_{,\theta\theta} = -2\psi \mathbf{u},$$

$$\mathbf{u}_{,\theta\theta} = \mathbf{x}_{,\psi\theta\theta} = -\mathbf{u}, \quad \mathbf{v}_{,\theta\theta} = \mathbf{x}_{,\theta\theta\theta} = -\mathbf{v}.$$

If we define E , F , and G by

$$E = \mathbf{u} \cdot \mathbf{u} = (\nabla\theta \cdot \nabla\theta)/B^2,$$

$$F = \mathbf{u} \cdot \mathbf{v} = -(\nabla\psi \cdot \nabla\theta)/B^2,$$

$$G = \mathbf{v} \cdot \mathbf{v} = (\nabla\psi \cdot \nabla\psi)/B^2,$$

we also have the following relations:

$$\mathbf{u} \cdot \mathbf{u}_{,\theta} = F/2\psi, \quad \mathbf{v} \cdot \mathbf{u}_{,\theta} = G/2\psi,$$

$$\mathbf{u} \cdot \mathbf{v}_{,\theta} = -2\psi E, \quad \mathbf{v} \cdot \mathbf{v}_{,\theta} = -2\psi F,$$

$$\mathbf{u} \cdot \mathbf{u}_{,\theta\theta} = -E, \quad \mathbf{v} \cdot \mathbf{u}_{,\theta\theta} = -F,$$

$$\mathbf{u} \cdot \mathbf{v}_{,\theta\theta} = -F, \quad \mathbf{v} \cdot \mathbf{v}_{,\theta\theta} = -G,$$

$$\mathbf{u}_{,\psi} \cdot \mathbf{u}_{,\theta} = -F/(2\psi)^2, \quad \mathbf{v}_{,\psi} \cdot \mathbf{u}_{,\theta} = G/(2\psi)^2,$$

$$\mathbf{u}_{,\psi} \cdot \mathbf{v}_{,\theta} = E, \quad \mathbf{v}_{,\psi} \cdot \mathbf{v}_{,\theta} = -F.$$

- [1] H. Hojo, M. Inutake, M. Ichimura, R. Katsumata and T. Watanabe, *Jpn. J. Appl. Phys.* **32**, 2116 (1993).
- [2] M. Inutake, A. Ishihara, R. Katsumata, M. Ichimura, A. Mase, K. Ishii, Y. Nakashima, Y. Nagayama, N. Yamaguchi, H. Hojo, I. Katanuma and T. Tamano, *Int. Conf. Open Plasma Confinement Systems for Fusion*, ed. A. Kabantsev (World Scientific, 1994), p.51.
- [3] X.S. Lee and P.J. Catto, *Phys. Fluids* **24**, 2010 (1981).
- [4] T.B. Kaiser and L.D. Pearlstein, *Phys. Fluids* **26**, 3053 (1983).
- [5] W.M. Nevins and L.D. Pearlstein, *Phys. Fluids* **31**, 1988 (1988).
- [6] D.A. D'Ippolite, B. Hafizi and J.R. Myra, *Phys. Fluids* **25**, 2223 (1982).
- [7] D.A. D'Ippolite and J.R. Myra, *Phys. Fluids* **27**, 2256 (1984).
- [8] B.I. Cohen, R.P. Freis and W.A. Newcomb, *Phys. Fluids* **29**, 1558 (1986).
- [9] W.A. Newcomb, *Phys. Fluids* **28**, 505 (1985).
- [10] H. Hojo, *Kakuyugo Kenkyu* **65**, 639 (1991) [in Japanese].
- [11] M.N. Rosenbluth and A. Simon, *Phys. Fluids* **8**, 1300 (1965).
- [12] H. Hojo, *J. Plasma Fusion Res.* **75**, 695 (1999).
- [13] M. Ichimura, R. Katsumata, M. Inutake, A. Ishihara, H. Hojo, I. Sasaki, K. Ishii, A. Mase, Y. Nakashima and T. Tamano, *Int. Conf. Open Plasma Confinement Systems for Fusion*, ed. A. Kabantsev (World Scientific, 1994), p.69.
- [14] A. Mase, A. Itakura, T. Tokuzawa, Y. Ito, H. Satake, H. Hojo, M. Ichimura, M. Inutake, K. Ishii, R. Katsumata and T. Tamano, *Int. Conf. Open Plasma Confinement Systems for Fusion*, ed. A. Kabantsev (World Scientific, 1994), p.211.